# AN AUTONOMOUS POLARIZED RAMAN LIDAR SYSTEM DESIGNED FOR SUMMIT CAMP, GREENLAND

**Robert A. Stillwell[1]*, Ryan R. Neely III[2,3], Peter Pilewskie[4], Michael O'Neill[3], Jeffrey P. Thayer[1], Matthew Hayman[5]**

*[1]Aerospace Engineering Sciences, University of Colorado, *Presenting Author, [2]School of Earth and Environment, University of Leeds, [3]Cooperative Institute for Research in Environmental Science, University of Colorado, [4]Atmospheric and Oceanic Sciences, University of Colorado, [5]Research Aviation Facility, National Center for Atmospheric Research*

## ABSTRACT

A dearth of high-spatial and temporal resolution measurements of atmospheric state variables in the Arctic directly inhibits scientific understanding of radiative and precipitation impacts on the changing surface environment. More reliable and frequent measurements are needed to better understand Arctic weather processes and constrain model predictions. To partially address the lack of Artic observations, a new autonomous Raman lidar system, which will measure water vapor mixing ratio, temperature, extinction, and cloud phase profiles through the troposphere, is designed for deployment to Summit Camp, Greenland (72° 36' N, 38° 25' W, 3250 [m]). This high-altitude Arctic field site has co-located ancillary equipment such as a Doppler millimeter cloud radar, microwave radiometers, depolarization lidars, ceiliometer, an infrared interferometer and twice-daily radiosondes. The current suite of instruments allows for a near comprehensive picture of the atmospheric state above Summit but increased spatial and temporal resolution of water vapor and temperature will reveal detailed microphysical information. A system description will be provided with an emphasis on the Monte Carlo safety analysis done to ensure eye safety in all relevant weather conditions.

## 1. INTRODUCTION

Unattended and automated lidar systems are becoming more common as atmospheric observational capabilities of lidar systems grow. Of particular interest for expanding observing capabilities are locations, which are historically undersampled due to the logistical challenges of maintaining an observational presence. The Greenland Ice Sheet is one such location due to its remote and extreme environment. Precipitative and radiative effects of tropospheric clouds and aerosols remain uncertain due to a lack of observations. High spatial and temporal resolution observations of temperature, water vapor mixing ratio, and cloud properties are needed. The Summit Polarized Raman Lidar (SuPR) is under construction to fill a vital gap in the current observational abilities of the Arctic Observing Network.

Using the Raman scattering technique, the unique rotational and vibrational structure of atmospheric constituents can be leveraged to uniquely identify species of interest. Combining that technique with polarization sensitivity yields more relevant cloud information but creates certain design challenges related to the trade of requirements and priorities.

## 2. SYSTEM DESIGN

The measurements that SuPR will make are split into three equally competing scientific goals: measurement of temperature, water vapor mixing ratio, and polarization properties of clouds and aerosols. Great care has been taken in the design phase to balance these three goals. By designing a Raman lidar system using the full Stokes Vector polarization treatment, one can accommodate the unique requirements of the three measurements. A system diagram of SuPR is given in Figure 1 with some relevant transmitter and receiver specifications given in Table 1.

Care has been taken with the system's polarization and physical alignment to allow for partially automated alignment procedures; this is helpful when considering the limited seasonal availability of the system. Extra optics as well as motorized mounts are included to perform automated polarization alignments.

By calculating the Mueller matrix of each element in the system and using it instead of scalar values, one could simulate the performance not only of the Raman returns but the systematic effects on the polarization measurements. Photon returns were calculated, using the Stokes Vector Lidar Equation, given in Equation 1.

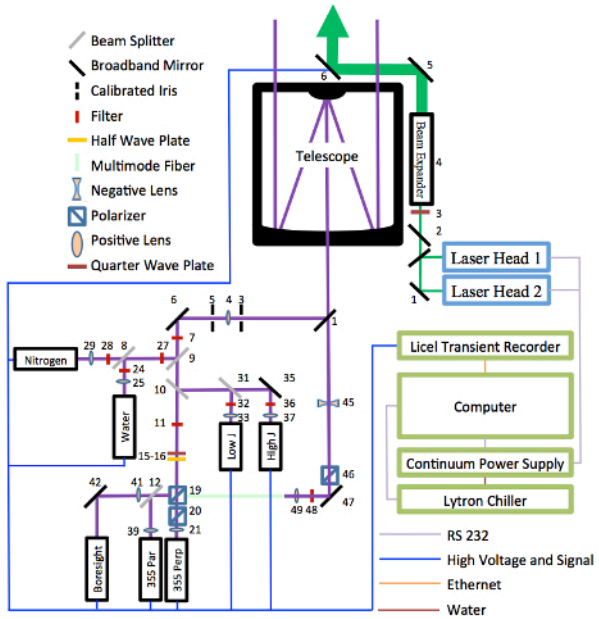


**Figure 1: A functional block diagram of the SuPR system. This design contains 4 Raman channels and two polarization sensitive channels.**

**Table 1: Relevant design specifications for SuPR.**

| Transmitter | Spec | Receiver | Spec |
|---|---|---|---|
| Divergence | 166 [μrad] | Aperture | 61 [cm] |
| Pulse Energy | 400 [mJ] | FOV | 252 [μrad] |
| Pulse Rate | 30 [Hz] | Filter Width | 0.3 [nm] |
| Polarization | Any | Resolution | 7.5 [m] |

$$\bar{N} = \bar{\bar{O}}\,\bar{\bar{M}}_{R_x}\left[\left(\bar{\bar{G}}\frac{A}{R^2}\Delta R\right)\bar{\bar{T}}_{atm}\bar{\bar{F}}\bar{\bar{T}}_{atm}\bar{\bar{M}}_{T_x}\bar{S}_{T_x} + \bar{S}_B\right] \quad (1)$$

Here, $\bar{S}_{T_x}$, $\bar{\bar{M}}_{T_x}$, $\bar{\bar{T}}_{atm}$, $\bar{\bar{F}}$, $\bar{\bar{M}}_{R_x}$, $\bar{\bar{G}}$, $\bar{\bar{O}}$, and $\bar{N}$ are the transmitted Stokes Vector, the Mueller matrix of the transmitter, Mueller matrices of atmospheric propagation, the Mueller matrix of scattering, the Mueller matrix of the receiver, the channel dependent overlap function, the matrix defining the observational channels, and the photon counts in those channels respectively. With those photon counts, retrievals were performed to estimate the measurement sensitivity. In the interest of brevity, only the retrievals are shown here. Because the atmosphere must be prescribed to determine raw photon counts, the exact value is known. This can be used to compare theoretical to retrieved values to determine measurement performance. This is done in Figure 2 for a 15-minute integrating period with temperature and water vapor profiles taken from Summit, measured by Vaisala radiosonde. These profiles are typical of what has been observed at Summit in early spring from a twice-daily radiosonde program. The background is taken from a UV spectrometer at Summit. Finally, a Poisson random number is used to simulate shot noise from photon counting.

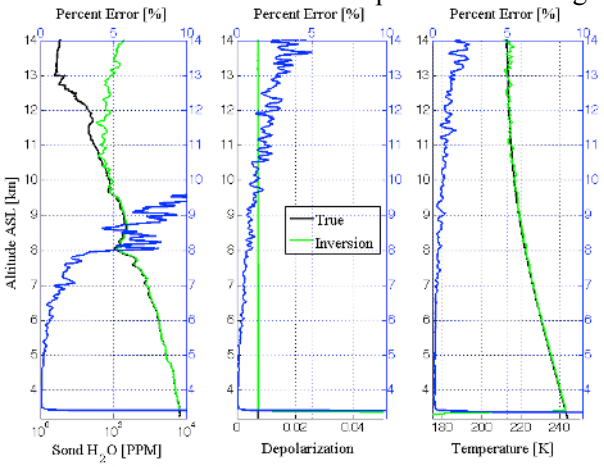


**Figure 2: Simulated retrievals for a 15-minute integration under background conditions observed at Summit during the summer-time (i.e. day time). The absolute anomaly is the percent error between the atmosphere modeled to simulate the raw signal and retrieved values. The resolution limit seen is a function of the high background modeled; the same simulation run during the winter-time (i.e. night time) yields similar resolution for polarization and temperature but increases the ability to retrieve water vapor mixing ratio to approximately 5 [PPM].**

## 3. EYE SAFETY

Due to the high energy density of pulsed lasers for Raman applications, burns are possible due to the fast heating of live tissue where the energy is accumulated much quicker than can be dissipated. To avoid this, the American National Standards Institute (ANSI) defines maximum permissible energy (MPE) levels for safe laser operation. These levels are based on pulse duration, peak power, repetition rate, and wavelength [1].

One major factor in the design effort for SuPR was the concern for eye safety. As the system is not designed to be deployed to a populated area, the accepted risks can be different than more traditional lidars. For example, the beam energy need not be below the MPE everywhere but the beam does need to have eye safe scattering in all conditions. There are many methods to meet the ANSI standards; among them are the use of low-power/high-repetition rate lasers, beam expansion [4], and the use of collocated surveillance radar [5]. For high-powered Raman lidar systems, the first is impractical, the second introduces cost and complexity due to the large expansions that are

often needed (possibly on the order of 10-20 times), and the third introduces complexity in incorporating such an ancillary system. Here, an accompanying method will be introduced which accounts for all relevant atmospheric absorption and scattering to ensure beam safety without introducing extra complexity or expense associated with the methods stated.

A Monte Carlo scattering model was created which accounts for atmospheric absorption and scattering to determine where a lidar beam is safe after propagation/scattering. This model will be applied to SuPR with weather conditions common at Summit but can be applied to other systems with different characteristics. In this case a fog example is given but the same simulations were run for clear air and blowing snow.

### 3.1 Monte Carlo Coordinate System

The method for defining scattering is in spherical coordinates where the phase function of a scatterer can be calculated directly from Mie theory for spheres and using ray tracing methods for non-spherical particles [3, 6]. The rotation matrix used to connect the propagation direction before and after scattering is given in Equation 2 where $\theta_i$ is the angle from zenith of scattering event $i$, $\phi_i$ is the azimuth angle of scattering event $i$, and C and S are cosine and sine respectively [2].

$$\boldsymbol{M_i} = \begin{bmatrix} \mathrm{C}(\theta_i)\,\mathrm{C}(\phi_i) & \mathrm{C}(\theta_i)\,\mathrm{S}(\phi_i) & -S(\theta_i) \\ -\mathrm{S}(\phi_i) & \mathrm{C}(\phi_i) & 0 \\ \mathrm{S}(\theta_i)\,\mathrm{C}(\phi_i) & \mathrm{S}(\theta_i)\,\mathrm{S}(\phi_i) & \mathrm{C}(\theta_i) \end{bmatrix} \quad (2)$$

The propagation direction, $\bar{\Omega}$, is:

$$\bar{\Omega}_i = [S(\theta_i)C(\phi_i) \quad S(\theta_i)S(\phi_i) \quad C(\phi_i)]^{\boldsymbol{T}} \quad (3)$$

The position of the photon, $\bar{\tau}$, is a function of the scattering directions $\theta_i$ and $\phi_i$ for each event, the number of total scattering events in the region of interest, n, and the optical depth traveled before the scattering event, $\tau_i$, and is given in Equation 4.

Using this method, the photon location can be tracked through a region of interest to find its exit position. This position can be summed into a discretized boundary to create a map of photon locations in optical depth space.

$$\bar{\tau} = \sum_{i=1}^{n} \tau_i \prod_{j=0}^{i-1} \boldsymbol{M_j^T}(\theta_j, \phi_j)\bar{\Omega}\,(\theta_i, \phi_i) \quad (4)$$

### 3.2 Scattering Characteristics

The three cases chosen for analysis represent three different methods of determining scattering characteristics as well as the three prominent weather patterns observed at Summit. Due to the coordinate systems defined, what is needed is the azimuthal and angle from zenith of any scattering event. The phase functions can be calculated exactly using Mie theory and ray tracing. Here, a geometric optics approach is assumed for ice. These exact phase functions can be converted using their normalized cumulative distribution function into a weighted random number. Using a random number and then comparing it to a cumulative distribution, a weighted random number can be created which is used in the Monte Carlo analysis to define scattering directions. This method is completely general, not limited to the phase functions used. An example is given for the fog case in Figure 3 which assumes a wavelength of 354.71 [nm] with scatterers defined by a gamma distribution of width parameter $\alpha = 7$ and effective radius of 10 [μm]. Similar steps can be completed for both the blowing snow case and clear air. For the blowing snow case, the phase function is from an assumed mix of roughened crystal habits of effective radius 30 μm [6], typical of what has been observed at Summit; for the clear air case, the phase function is derived directly from dipole (molecular) scattering.

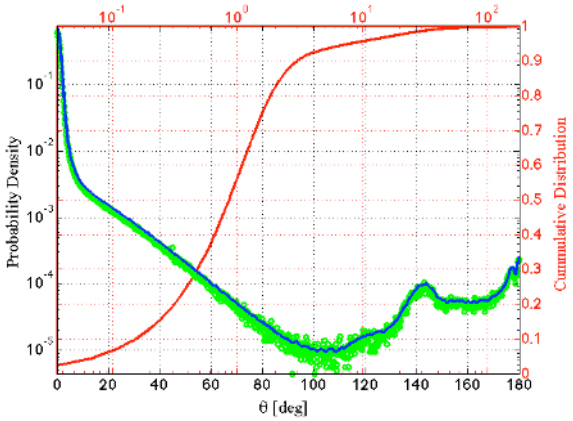


**Figure 3: A phase function for spherical fog droplets. The exact solution from Mie theory is the solid blue line, the Monte Carlo approximation using $10^7$ particles with 1000 bin discretization in green dots, and the cumulative distribution function used to convert to weighted random numbers in red. Note the top abscissa is logarithmic.**

### 3.3 Energy Maps

Given a region of interest around the lidar beam, a map of energy density is calculated which is then compared to relevant MPE values. The region of interest is defined as a cylinder around the beam with a set radius, r, and height, h. That

region is then converted from units of distance to optical depth. This requires knowledge of the optical depth per meter, which is different for all three cases. For air, a simple Rayleigh scattering extinction model suffices. For water and ice particle scattering, optical depth can be calculated from the knowledge of particle size distribution, $n(r)$, density, $\rho$, effective radius, $r_e$, and liquid water path, $LWP$. This conversion is given in Equation 5.

$$r_e = \frac{\int_0^\infty r^3 n(r) dr}{\int_0^\infty r^2 n(r) dr} = \frac{3}{2}\frac{LWP}{\rho\tau} \quad (5)$$

The following results are for the phase function in Figure 3. The system parameters given in Table 1 are all simulated which yields a multipulse MPE of 1.23 [mJ/cm$^2$]. This map is given in Figure 4.

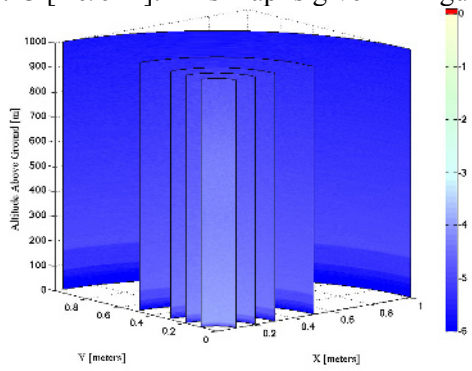


**Figure 4: Log$_{10}$ energy density in [mJ/cm$^2$] caused by fog scattering. This map shows the intensity as a function of radius for 10, 20, 30, 50, and 100 cm. Red is in excess of the MPE; the direct beam is the only source intense enough to exceed the MPE at 355 [nm]. However, the energy is very near the MPE for 532 [nm].**

The impact of the direct beam and forward scattering is evident in Figure 5.

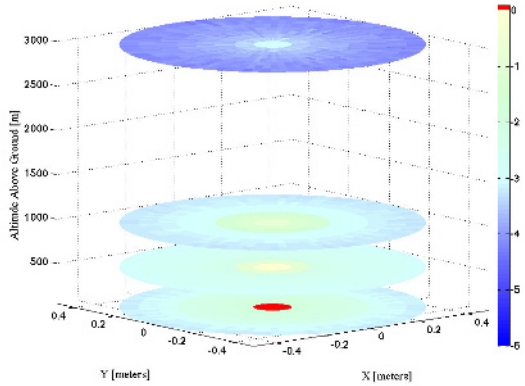


**Figure 5: Log$_{10}$ energy density in [mJ/cm$^2$] at four altitudes. Red is in excess of the MPE. Monte Carlo simulations are run with 10$^7$ photons and show no beam hazards outside of the direct beam below aircraft flight altitude in foggy conditions.**

## 4. CONCLUSIONS

The work shown here provides a design for an Arctic Raman/Polarization lidar system. The system designed meets its three pronged scientific requirements of measuring water vapor, temperature and polarization properties through the troposphere in all background conditions. Furthermore, a detailed atmospheric scattering simulation was performed to test eye safety concerns in inclement weather. Shown were the results from diurnally forced fog events, which show that the only hazard is the direct beam. Other simulations that include blowing snow and clear air scattering also yielded similar results. The beam is safe at 355 [nm] but given the same system at 532 [nm], scattered energy in excess of the MPE is readily observable with this design. It should also be noted that these results could also be applied to address lidar observations under multiple scattering conditions.

## ACKNOWLEDGEMENT

This material is based upon work supported by the National Science Foundation Graduate Research Fellowship under Grant No. DGE 1144083 and National Science Foundation Grant No. AON 1303864.

## REFERENCES

[1] American National Standard for Safe Use of Lasers (ANSI Z136.1). Laser Institute of America, 2013.

[2] Bohren, C. F. and E. E. Clothiaux. Fundamentals of Atmospheric Radiation. Wiley-VCH Verlag GmbH and Co. KGaA, 2005.

[3] Bohren, C. F. and D.R. Huffman. Absorption and Scattering of Light by Small Particles. Wiley-VCH Verlag GmbH and Co. KGaA, 1998.

[4] Radlach, M. et al. Scanning rotational Raman lidar at 355 nm for the measurement of tropospheric temperature fields. Atmos. Chem. Phys., 8, 159-169, 2008.

[5] Thayer, J. P. et al. Rayleigh lidar system for middle atmosphere research in the arctic. Opt. Eng. 36, 2045-2061. 1997.

[6]Yang, P., L. Bi, B. A. Baum, K.-N. Liou, G. Kattawar, and M. Mishchenko, 2013: Spectrally consistent scattering, absorption, and polarization properties of atmospheric ice crystals at wavelengths from 0.2 µm to 100 µm. *J. Atmos. Sci*., 70, 330-347.